Microstructure and mechanical properties of Al–Mg–Er sheets jointed by friction stir welding

H.L. Hao, D.R. Ni, Z. Zhang, D. Wang, B.L. Xiao *, Z.Y. Ma

Shenyang National Laboratory for Materials Science, Institute of Metal Research, Chinese Academy of Sciences, Shenyang 110016, China

A B S T R A C T

1.7 mm thick cold-rolled Al–Mg–Er alloy sheets under as-rolled and annealed conditions were subjected to friction stir welding (FSW). The as-rolled sheet showed fibrous tissues with a high density of dislocations. After annealing, the fibrous tissues were replaced by coarse, nearly-equiaxed grains ∼18 µm in size and the density of dislocations decreased greatly, resulting in significantly reduced hardness of the annealed sheet. After FSW, the nugget zone (NZ) of both the FSW joints of as-rolled and as-annealed sheets consisted of fine equiaxed recrystallised grains with sizes of 4.5 µm and 4.3 µm, respectively. For the joint of the as-rolled sheet, the dislocations in the NZ and thermomechanically affected zone (TMAZ) were significantly reduced and the NZ showed lower hardness than the base material (BM). However, for the joint of the as-annealed sheet, the NZ exhibited higher hardness than the BM due to significant grain refinement in the NZ. The joint of the as-rolled sheet showed a joint efficiency of 68% and fractured in the NZ but the joint of the as-annealed sheet had a joint efficiency of nearly 100% and fractured in the BM.

© 2013 Elsevier Ltd. All rights reserved.

1. Introduction

Aluminium alloys are generally classified into precipitation-hardened alloys and solid-solution-hardened alloys. 5××× alloys are widely used in transportation and shipbuilding industries. As solution-hardened alloys, they can be strengthened only by work hardening and/or by microalloying [1,2] and magnesium is the principal alloying element.

The addition of rare earth elements would provide the aluminium alloys with some novel benefits. For example, the addition of scandium (Sc) can improve the mechanical properties and corrosion resistance of the aluminium alloys [3,4] and it can also eliminate the influence of harmful impurity, playing a purification role [5]. However, the use of Sc is limited due to its high cost. Compared with Sc, erbium (Er) offers similar functions and is much cheaper. Xing et al. [6] concluded that Er enhanced the tensile strength of a cast Al–Mg alloy without greatly decreasing the elongation, due to the formation of many fine primary and precipitation Al_3Er particles. Al_3Er particles have a coherent relationship with the matrix phase alpha-Al, which can be acted as the heterogeneous nucleus and the other hands it can strongly pin up dislocations and subgrain boundaries and retard the recrystallization of alloys. Nie et al. [7] also reported similar results for Al–5Mg alloys. Therefore, Al–Mg–Er alloys offer a wide development potential [8].

The sound welding of Al–Mg–Er alloys is important and necessary for their wide application. Although several investigations have reported on this aspect in recent years, they focused only on fusion welding techniques. Li [9] welded a cast Al–Mg–Er alloy plate using traditional tungsten inert gas arc welding (TIG) and laser welding (LW) methods. It was reported that the ultimate tensile strength (UTS) and yield strength (YS) of the joints were 80% and 50% of the BM which fractured in the heat affected zone for the TIG and 75% and 60% of the BM which fractured in the weld zone for the LW, respectively. However, for the welding of aluminium alloys, traditional fusion welding methods are apt to generate porosity, cavities, hot cracking and solidification and liquation cracking [1,8,10].

As a solid-state joining process, friction stir welding (FSW) may avoid the problems encountered during traditional fusion welding [11,12]. Furthermore, FSW has several prominent beneficial features, such as energy efficiency, environmental friendliness and versatility [13–17] and there is no need for surface cleaning operations prior to the FSW process [18–20]. FSW has been proved to be successful for a great number of aluminium alloys. However, to the best of the authors' knowledge, no research has been reported to date on the FSW of Al–Mg–Er alloys.

In this study, the 1.7 mm thick cold-rolled Al–Mg–Er sheets were subjected to FSW before and after annealing. The aim was to evaluate the FSW weld-ability of the thin Al–Mg–Er sheets and to examine the effects of the initial state of the Al–Mg–Er sheets on the mechanical properties of the FSW joints.

* Corresponding author. Tel./fax: +86 24 83978630.
  E-mail address: blxiao@imr.ac.cn (B.L. Xiao).

2. Experimental details

1.7 mm thick cold-rolled sheets of Al–5.7Mg–0.6Mn–0.1Zr–0.3Er (wt.%) were used in this study. Parts of the sheets were annealed at 300 °C for 2 h. Both the as-rolled and as-annealed sheets (hereafter referred to as as-rolled and as-annealed sheets) were subjected to FSW along the rolling direction at a rotation rate of 400 rpm and a welding speed of 100 mm/min. A steel tool with a shoulder 12 mm in diameter and a threaded cylindrical pin 4 mm in diameter and 1.4 mm in length was used. A tilting angle of 2.5° was used for all the FSW processes and the plunge depth of the shoulder was controlled at ~0.15 mm.

In order to reveal the grain microstructure, initially the FSW joints were artificially aged at 120 °C for 16.5 h to decorate the grain boundaries and then cross-sectioned perpendicular to the FSW direction. The sectioned specimens were polished and then etched with a solution of 10 mL phosphoric acid and 90 mL water at 80 °C.

The macrostructure and microstructure of the FSW joints were observed by stereoscopy and optical microscopy (OM, Axiovert 200 MAT). The distribution of precipitates and dislocations were characterised by transmission electron microscopy (TEM, TECNAI 20). Thin discs for TEM observations were cut from various locations throughout the welds and the base metal (BM). Thin foils were prepared by jet electro-polishing with a solution of nitric acid (1/3) and methanol (2/3) at −30 °C. Phase identification was conducted via X-ray diffractometry (XRD) with Cu Kα radiation.

Vickers hardness and tensile tests were conducted in accordance with ASTM: E384-11e1 (Standard Test Method for Knoop and Vickers Hardness of Materials) and ASTM: E8/E8M-11 (Standard Test Methods for Tension Testing of Metallic Materials), respectively. Vickers hardness profiles were measured on the cross-section perpendicular to the welding direction along the mid-thickness of the sheets using a computerised Buehler hardness tester under a load of 100 g for 10 s. Transverse tensile specimens with a gauge length of 40 mm and a width of 10 mm were machined perpendicular to the FSW direction. Room temperature tensile tests were carried out at a strain rate of $6 \times 10^{-4} \, \mathrm{s}^{-1}$ and three specimens were tested for each group. The failed specimens were observed under a stereoscope and the fracture surfaces examined under a Quanta 600 scanning electron microscope (SEM).

3. Results and discussion

3.1. Microstructures

Fig. 1 shows the cross-sectional macrographs of the FSW joints. No defects were detected in either of the FSW joints. Based on the microstructural characterisation, four zones, i.e.: the BM, the heat affected zone (HAZ), the thermomechanically affected zone (TMAZ) and nugget zone (NZ) were identified in the joints. In the FSW joint of the as-rolled sheet, there existed a "line S" as shown by the arrow (Fig. 1a). The "line S" is believed to originate from the oxide layer on the initial butt surfaces, which was broken up, extruded and deformed during FSW [21,22]. In the weld of the as-rolled
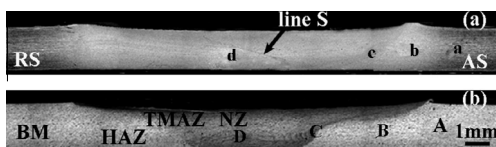
sheet, the boundary around the NZ was not clear (Fig. 1a). However, the boundary became distinct in the weld of the as-annealed sheet (Fig. 1b).

Fig. 2 shows the microstructures of the joints at the locations "a", "b", "c" and "d" of Fig. 1a, which represent the microstructures of the BM, HAZ, TMAZ and NZ of as-rolled sheet, respectively. The microstructure of the as-rolled BM was characterised by fibrous tissues of elongated grains (Fig. 2a). In the HAZ (Fig. 2b), equiaxed grains developed and the average grain size was determined to be ~12 μm. This indicates that recrystallisation occurred in the HAZ. It is known that the HAZ did not undergo any plastic deformation and just experienced a thermal cycle during FSW [23]. Therefore, static recrystallisation, which was assisted by high deformation energy stored during cold rolling [24], took place in the HAZ.

As shown in Fig. 2c, the TMAZ did not show the typical characteristics of elongated grains normally observed in FSW joints of Al–Mg alloys [25,26]. This region was characterised by equiaxed recrystallised grains with average grain size (~7.2 μm) similar to that of the NZ's boundary. Etter et al. [24] considered that continuous dynamic recrystallisation occurred and no geometric dynamic recrystallisation happened in the TMAZ of the as-rolled sheet. Therefore, no typical TMAZ microstructure was observed in the joint of the as-rolled sheet and thus, the outline of the NZ was indistinct. The NZ had fine, equiaxed recrystallised grains with an average size of ~4.5 μm (Fig. 2d). The fine equiaxed grains in the NZs were attributed to the dynamic recrystallisation caused by the intense plastic deformation and the frictional heat arising from the rotating tool [24].

Fig. 3 shows the microstructures of the joints at the locations "A", "B", "C" and "D" of Fig. 1b. Regions A through D correspond to the BM, HAZ, TMAZ and NZ of the as-annealed sheet, respectively. After annealing, the elongated grains changed into coarse nearly-equiaxed grains due to the recovery and recrystallisation and the average grain size was ~18 μm (Fig. 3a). The microstructure of the HAZ (Fig. 3b) was slightly coarsened compared with that of the BM and the average grain size was ~22 μm. The TMAZ was characterised by the typical microstructure of the elongated grains. The NZ had fine, equiaxed recrystallised grains and the average grain size was ~4.3 μm (Fig. 3d).

The XRD patterns (Fig. 4) showed the presence of Al₃Er, Mg₂Si and Al₆Mn phases in both the NZs and BMs of both the as-rolled and as-annealed sheets. The SEM images showed the variation of second phase particle size and distribution in various regions of the FSW joints (Fig. 5). The BMs (Fig. 5a and d) of the as-rolled and as-annealed sheets were shown to contain Mg_2Si, Al_3Er and Al_6Mn through the analysis of EDS. The Mg_2Si particles dissolve at about 525 °C. The Al_6Mn particles dissolve at about 600 °C, which is above the temperatures reached during FSW. The Al_3Er has high thermal stability with a melting temperature of 1067 °C. The high temperature and severe plastic deformation caused by the FSW process could result in the dissolution, growth and break-up of these second phase particles [27]. This combined effect led to the change of particles after welding. Therefore, the average sizes of Al_3Er, Mg_2Si and Al_6Mn in the TMAZ and NZ were smaller than those in the BM due to the breakup effect. Moreover, the volume fraction of Mg_2Si was reduced after welding due to the dissolution of Mg_2Si. The particles in the TMAZ (Fig. 5b and e) were distributed along the flow direction of the material.

TEM observations showed that a high density of dislocations was observed in the as-rolled BM (Fig. 6a). This is associated with the condition of the cold-rolled sheet. After FSW, only a few dislocations were observed in the TMAZ (Fig. 6b) and no dislocations existed in the NZ (Fig. 6c). This is attributed to the annealing effect caused by FSW. Compared with the as-rolled BM, little dislocations were observed in the as-annealed BM (Fig. 6d). However, dislocations could be found in both the TMAZ (Fig. 6e) and the NZ
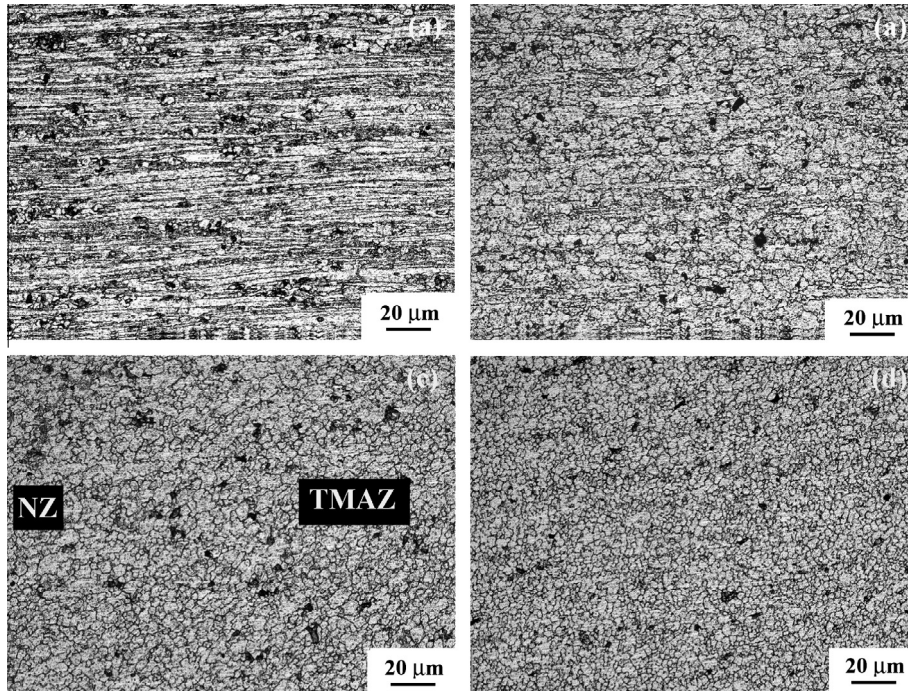

Fig. 1. Cross-sectional macrographs of Al–Mg–Er joints of (a) as-rolled sheet and (b) as-annealed sheet.

Fig. 2. Microstructures of positions "a", "b", "c" and "d" in Fig. 1a.
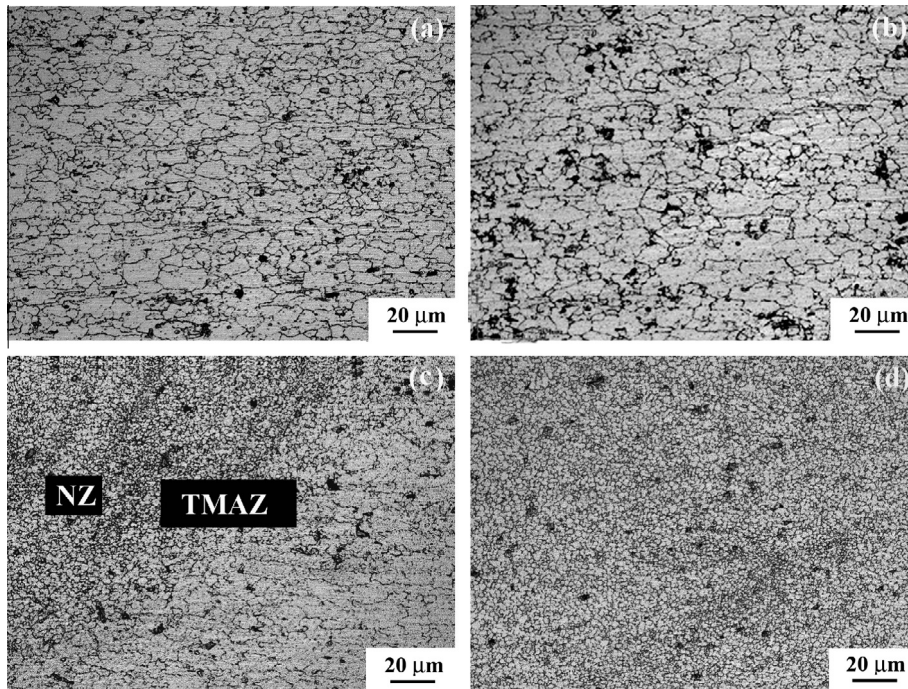

Fig. 3. Microstructures of positions "A", "B", "C" and "D" in Fig. 1b.

(Fig. 6f) for the annealed sheet. According to the selected area diffraction patterns (Fig. 6b and d), it was found that nano-sized Al_3Er particles (as shown by the arrows) existed in the BM, the TMAZ and the NZ under the various conditions.

3.2. Microhardness

Fig. 7 shows the hardness profiles of the two FSW joints along the mid-thickness of the transverse cross-section. The hardness profiles were almost symmetric on the advancing side (AS) and the retreating side (RS). For the as-rolled sheet, the hardness started to decrease in the HAZ, due to the annealing softening and static recrystallisation (Fig. 2c) that reduced the effect of the work hardening. The NZ had the lowest hardness compared with the BM with hardness values decreasing from 130 to 87 Hv. This could be attributed to significant annealing softening and dynamic recrystallisation [27]. Compared with the as-rolled BM, the hardness of as-annealed BM dramatically decreased and this could be attributed to the decrease of the dislocation density due to the annealing [28] (Fig. 6a and d).
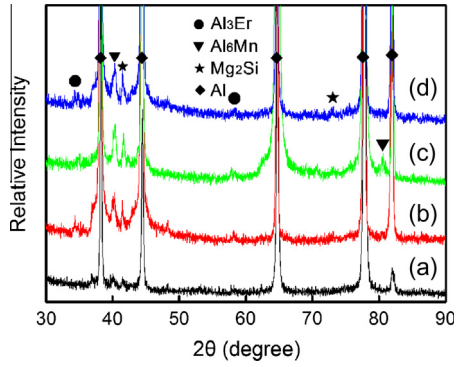
Fig. 4. XRD patterns of (a) as-rolled sheet, (b) NZ of as-rolled sheet, (c) as-annealed sheet, and (d) NZ of as-annealed sheet.

For the as-annealed sheet, the hardness of the HAZ was similar to that of the BM. This is attributed to the nearly same grain size between the HAZ and BM (Fig. 3a and b). The NZ showed the highest hardness compared with its BM with hardness values increasing from 83 to 95 Hv. The hardness change of the NZs is attributed to the following reasons. Firstly, the finer grains increased the hardness of the NZ. According to the Hall–Petch relationship and the model of Sato et al. [27], if the grain size decreased from 18 to 4.3 μm, the hardness could increase by about 4.5 Hv. This accounts for more than one third of the hardness difference between the NZ and BM. Secondly, the increased dislocation density in the NZ also resulted in the increase of hardness (Fig. 6f). Thirdly, the solid-solution strengthening of Mg atoms can also affect the hardness of the Al–Mg–Er sheet because the introduced dislocations can be locked by Mg atoms [29,30]. Attallah et al. [31] considered that the existing Mg$_2$Si particles were dissolved in the NZ during FSW and that this
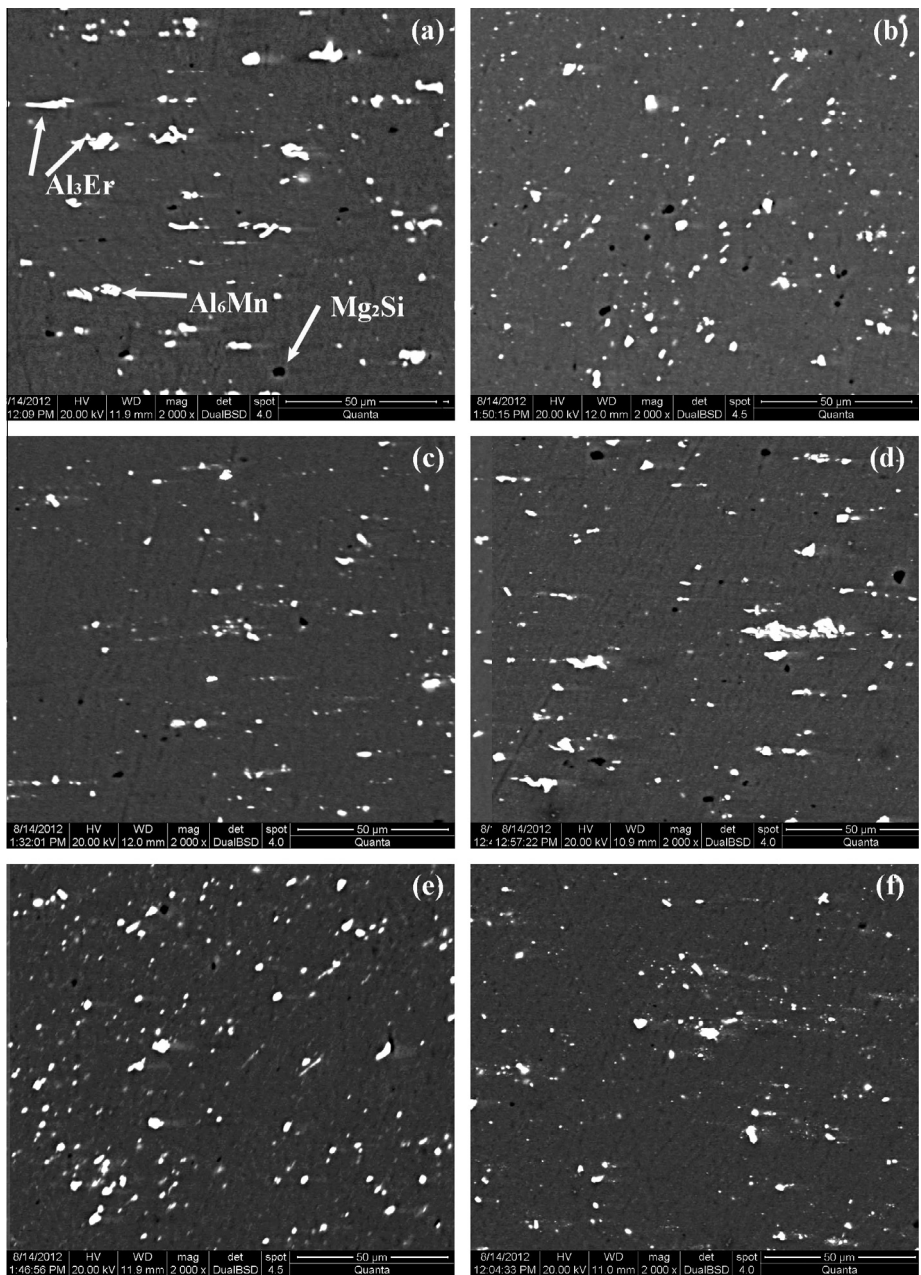

Fig. 5. Microstructures of (a) as-rolled sheet, (b) TMAZ in joint of as-rolled sheet, (c) NZ in joint of as-rolled sheet; (d) as-annealed sheet, (e) TMAZ in joint of as-annealed sheet and (f) NZ in joint of as-annealed sheet.
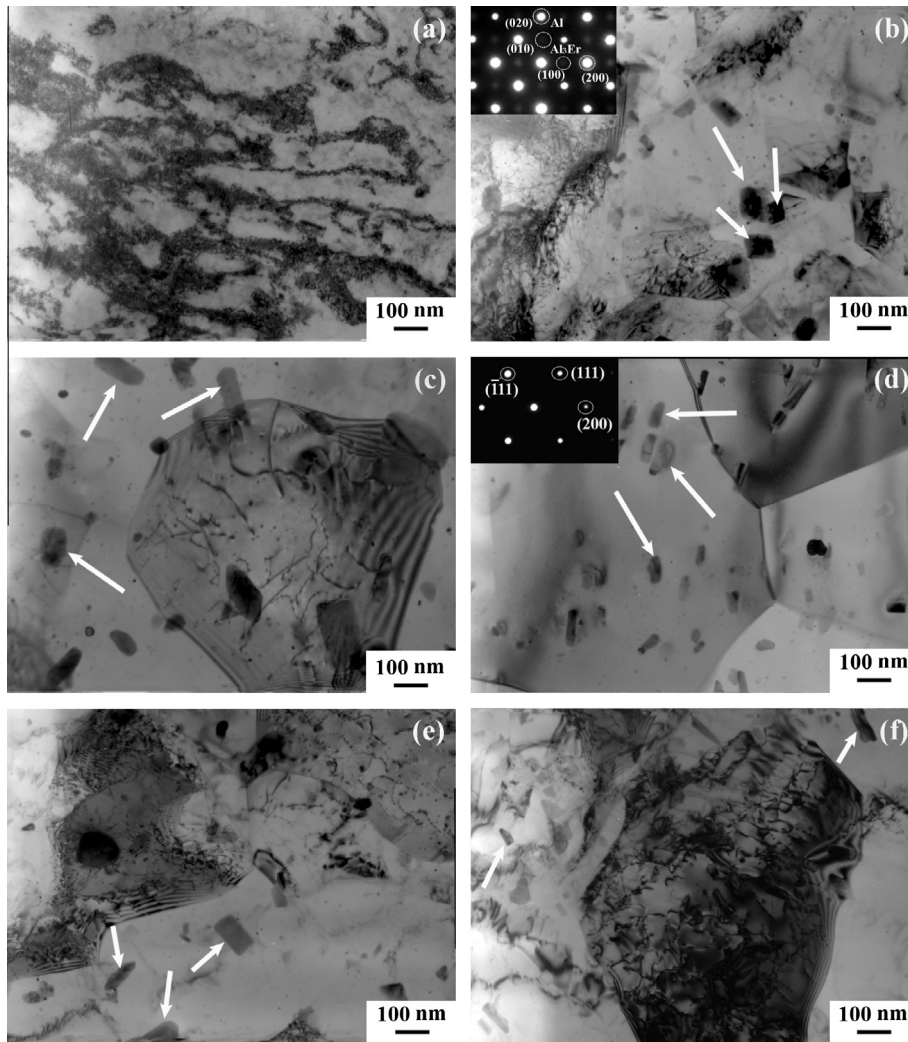
Fig. 6. Bright field TEM micrographs: (a) as-rolled sheet, (b) TMAZ in joint of as-rolled sheet, (c) NZ in joint of as-rolled sheet; (d) as-annealed sheet, (e) TMAZ in joint of as-annealed sheet and (f) NZ in joint of as-annealed sheet.
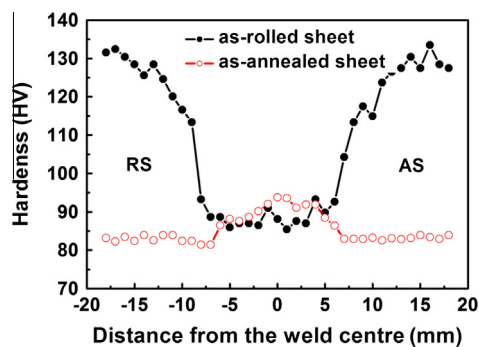

Fig. 7. Hardness profiles of FSW joints of as-rolled sheet and as-annealed sheet.

dissolution increased the Mg content in the solid solution, leading to the increase of the hardness in the NZ. Fourthly, for the as-annealed sheet, the volume fraction of particles decreased. According to the Orowan mechanism, this change would lead to a decrease of hardness. The combined effect of these four factors resulted in the increase of hardness in the NZ.

Figs. 8 and 9 show the top and side views of the failed tensile samples, respectively. The BMs of both sheets fractured randomly in the parallel part and showed slight necking. Both the two FSW joints fractured in the lowest hardness region; namely, the joint of the as-rolled sheet fractured in the NZ, while the joint of the as-annealed sheet fractured in the BM. The FSW joint failed with obvious necking occurring near the fracture location for the as-rolled sheet. The FSW joints of both the as-rolled sheet and the as-annealed sheet did not fracture along the line "S". This indicates that the line "S" would not show significant effect on the mechanical properties of the joints. Schneider and Nunesd [21] and Ren et al. [22] also reported similar results.

3.3. Tensile properties

The tensile properties of the BMs and FSW joints are shown in Table 1. For the joint of the as-rolled sheet, the YS, UTS and elongation decreased in contrast with those of the BM and were about 48%, 68% and 83%, respectively of that of the BM. The significant reduction of the tensile properties was due to the annealing softening and recrystallisation (Fig. 4a–c). The YS (173 MPa) and UTS (322 MPa) of the as-annealed sheet were greatly reduced compared with those of the as-rolled sheet, and were only 41% and 66%, respectively of those of the as-rolled sheet. This was because the as-rolled sheet was in a cold-working state with high density of dislocations (Fig. 6a), resulting in the high strengths. After anneal-
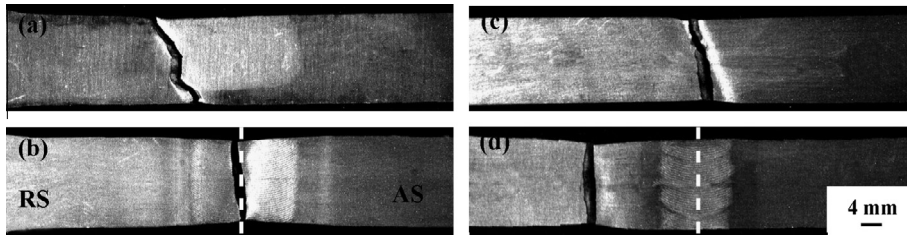
Fig. 8. Top view of failed tensile specimens: (a) as-rolled sheet, (b) joint of as-rolled sheet, (c) as-annealed sheet and (d) joint of as-annealed sheet.
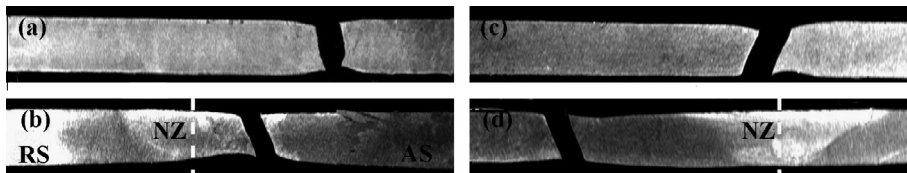

Fig. 9. Side views of failed tensile specimens: (a) as-rolled sheet, (b) joint of as-rolled sheet, (c) as-annealed sheet and (d) joint of as-annealed sheet.

Table 1
Tensile properties of BMs and FSW joints of Al–Mg–Er alloy.

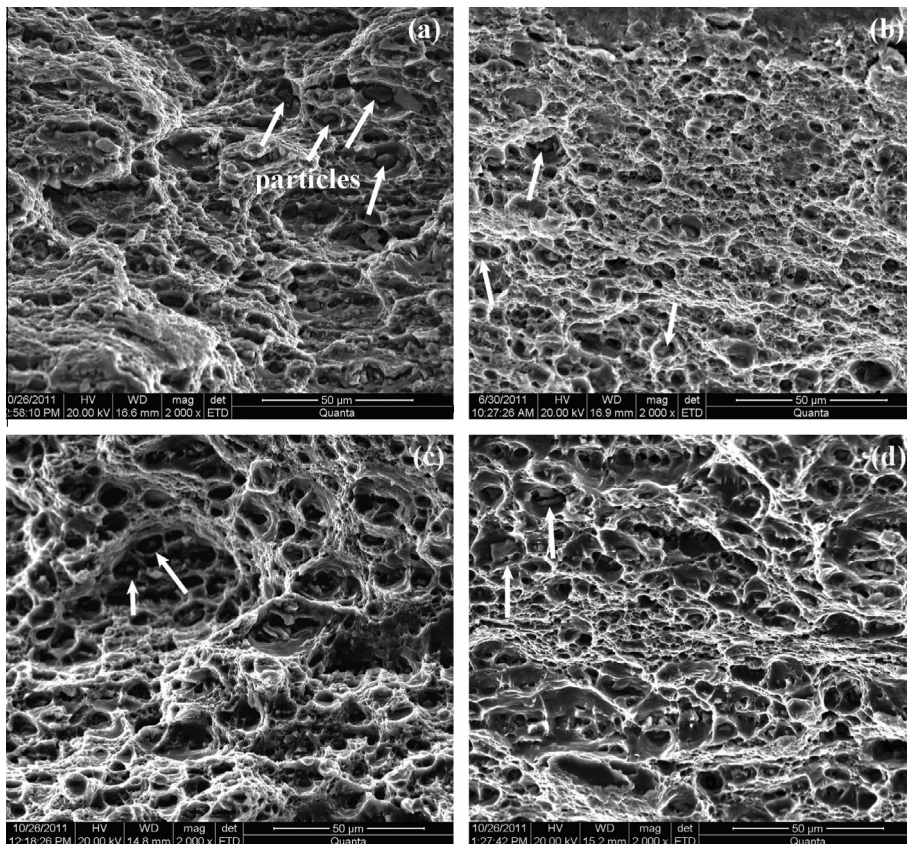|	YS (MPa)	UTS (MPa)	Elongation (%)	Joint efficiency (%)
As-rolled BM	423 ± 2.3	489 ± 2.5	9.5 ± 0.8	
FSW joint	203 ± 5.5	331 ± 8.0	7.9 ± 0.7	67.6
As-annealed BM	173 ± 3.1	322 ± 1.7	22.6 ± 0.5	
FSW joint	162 ± 0.5	314 ± 2.6	17.9 ± 1.2	97.3

Fig. 10. SEM fractographs of (a) as-rolled sheet, (b) joint of as-rolled sheet, (c) as-annealed sheet and (d) joint of as-annealed sheet.

ing, the dislocations were reduced dramatically, such that the YS and UTS decreased.

For the as-annealed sheet, the joint showed only slightly reduced YS and UTS compared with the BM and they were about 93% and 97%, respectively of that of the BM. However, the elongation was reduced to 79% of that of the BM. Nearly 100% of the joint efficiency was attributed to the higher hardness of the NZ resulting from the refined grains (Fig. 3b and d) and the increased dislocations (Fig. 6d and f).

For the TIG and LW joints of the cast Al–Mg–Er [9], internal flaws such as porosity and slag inclusion could be generated, which deteriorated the mechanical properties of the joints: the joint efficiencies were 80% for TIG and 75% for LW, respectively. However, no defects were found in the FSW joints of the cold-rolled Al–Mg–Er alloy in the present study. Moreover, for the as-annealed sheet, its joint efficiency could reach as high as 97%.

3.4. Fracture surface

Fig. 10 shows the fracture surfaces of the failed BMs and joints. The fracture surface of as-rolled BM (Fig. 10a) contained small inhomogeneous dimples and cleavage planes indicating the mode of mixed fracture. The fracture also contained many particles as shown by the arrows. The fracture surface of the joint of the as-rolled sheet (Fig. 10b) exhibited small-sized dimples with bits of fine particles, which were consistent with finer second phase particles in the NZ (Fig. 5c). Compared with the as-rolled BM, the fracture surface of the as-annealed sheets was covered by fine homogeneous dimples with some particles being detected (Fig. 10c). This indicates that the as-annealed sheet failed in the mode of ductility and possessed better ductility than the as-rolled sheet. The fracture surface of the joint of the as-annealed sheet (Fig. 10d) showed little difference from that of the BM, because the joint also fractured in the BM.

4. Conclusions

Sound FSW joints of 1.7 mm thick Al–Mg–Er sheets under as-rolled and as-annealed conditions were successfully produced. For the joint of the as-rolled sheet, the TMAZ did show the typical characteristics of elongated grains and the fine equiaxed recrystallised grain size of the NZ was 4.5 μm. For the joint of the as-annealed joint, the TMAZ showed the typical microstructure of elongated grains and the grain size of the BM and the NZ were 18 and 4.3 μm, respectively.

The as-rolled BM had a high density of dislocations. Following FSW, the dislocations dramatically decreased in the NZ and TMAZ. Few dislocations were observed in the as-annealed BM but following FSW, some dislocations appeared in the NZ and TMAZ.

For the as-rolled sheet, the hardness of the NZ was decreased from 130 to 87 Hv and the YS and UTS of the joint were 48% and 68%, respectively of that of the BM. However, for the as-annealed sheet, the hardness of the NZ increased from 83 to 95 Hv and the YS and UTS of the joint were 94% and 97%, respectively of that of the BM.

Acknowledgments

References

[1] Zhou H, Rao M, You W. The effect of element Er and Sc on the properties of Al–60Mg alloy. Aluminum Process 2011;1:4–13.

[2] Zhou CZ, Yang XQ, Luan GH. Fatigue properties of friction stir welds in Al 5083 alloy. Scripta Mater 2004;53:1187–91.

[3] Cabello Munoza A, Rückert G, Huneau B, Sauvage X, Marya S. Comparison of TIG welded and friction stir welded Al–45Mg–0.26Sc alloy. J Mater Process Technol 2008;197:337–43.

[4] Cavaliere P, Cabbile M. Effect of Sc and Zr addition on the microstructure and fatigue properties of AA6106 produced by equal-channel-angular-pressing. Mater Charact 2008;59:197–203.

[5] Cui GR, Ma ZY, Li SX. The origin of non-uniform microstructure and its effects on the mechanical properties of a friction stir processed Al–Mg alloy. Acta Mater 2009;57:5718–29.

[6] Xing ZB, Nie ZR, Zou JX, Ji XL, Wang XD. Effect of trace element Er on Al–Mg and Al–Mg–Mn alloys. Mater Sci Forum 2007;546:899–904.

[7] Nie ZR, Wang W, Jin TN, Huang H, Li MH, Zou JX, et al. Study on the erbium strengthened aluminum alloy. Mater Sci Forum 2007;546–549:623–8.

[8] Rosalbino F, Angelini E, De Negri S, Saccone A, Delfino S. Influence of the rare earth content on the electrochemical behaviour of Al–Mg–Er alloys. Intermetallics 2003;11:435–41.

[9] Li CY. Effect of welding parameters on microstructure and mechanical properties of Al–Mg–Er alloys. China: Beijing University of Technology; 2010.

[10] Jayaraman M, Sivasubramanian R, Balasubramanian V, Babu S. Influence of process parameters on tensile strength of friction stir welded cast A319 aluminium alloy joints. Metal Mater Int 2009;15:313–20.

[11] Rajakumar S, Muralidharan C, Balasubramanian V. Establishing empirical relationships to predict grain size and tensile strength of friction stir welded AA 6061–T6 aluminium alloy joints. Trans Nonferrous Metals Soc China 2010;20:1863–72.

[12] Kumbhar NT, Sahoo SK, Samajdar I, Dey GK, Bhanumurthy K. Microstructure and microtextural studies of friction stir welded aluminium alloy 5052. Mater Des 2011;32:1657–66.

[13] Elangovan K, Balasubramanian V. Influence of tool pin profile and tool shoulder diameter on the formation of friction stir processing zone in AA6061 aluminium alloy. Mater Des 2008;29:362–73.

[14] Singh RKR, Sharma C, Dwivedi DK, Mehta NK, Kumar P. The microstructure and mechanical properties of friction stir welded Al–Zn–Mg alloy in as wedled and heat treated conditions. Mater Des 2011;32:682–7.

[15] Xie GM, Ma ZY, Geng L. Effect of Y addition on microstructure and mechanical properties of friction stir welded ZK60 alloy. J Mater Sci Technol 2009;125:351–5.

[16] Munoz AC, Rückert G, Huneau B, Sauvage X, Marya S. Process technol comparison of TIG welded and friction stir welded Al–4.5Mg–0.26Sc alloy. J Mater Process Technol 2008;197:337–43.

[17] Chen TP, Lin WB. Optimal FSW process parameters for interface and welded zone toughness of dissimilar aluminum–steel joint. Sci Technol Weld Joining 2010;15:279–85.

[18] Silva AAM, Arruti E, Janeiro G, Aldanondo E, Alvarez P, Echeverria A. Material flow and mechanical behaviour of dissmilar AA2024-T3 and AA7075-T6 aluminium alloys friction stir welds. Mater Des 2011;32:2021–7.

[19] Elangovan K, Balasubramanian V, Valliappan M. Effect of tool pin profile and tool rotational speed on mechanical properties of friction stir welded AA6061 aluminium alloy. Mater Manuf Process 2008;23:251–60.

[20] Rodrigues DM, Leita C, Louro R, Gouveia H, Loureiro A. High speed friction stir welding of aluminium alloys. Sci Technol Weld Joining 2010;15:676–81.

[21] Schneider JA, Nunesd AC. Characterization of plastic flow and resulting microtextures in a friction stir weld. J Metall Mater Trans B 2004;35:777–83.

[22] Ren SR, Ma ZY, Chen LQ. Effect of initial butt surface on tensile properties and fracture behavior of friction stir welded Al–Zn–Mg–Cu alloy. Mater Sci Eng A 2008;479:293–9.

[23] Mishra RS, Ma ZY. Friction stir welding and processing. Mater Sci Eng 2005;50:1–78.

[24] Etter AL, Baudin T, Fredj N, Penelle R. Recrystallization mechanisms in 5251 H14 and 5251 O aluminum friction stir welds. Mater Sci Eng A 2007;445:94–9.

[25] Genevois C, Denquin A, Doisneau-cottignies B. Quantitative investigation of precipitation and mechanical behaviour for AA2024 friction stir welds. Acta Mater 2005;53:2447–58.

[26] Fratini L, BuffaG. CDRX modelling in friction stir welding of aluminium alloys. Int J Mach Tool Manuf 2005;45:1188–94.

[27] Sato YS, Park SHC, Kokawa H. Microtexture in the friction-stir weld of an aluminum alloy. Metall Mater Trans A 2001;32:3033–42.

[28] Flores OV, Kennedy C, Murr LE, Brown D, Pappu S, Nowak BM, et al. Microstructural issues in a friction stir welded aluminum alloy. Scripta Mater 1998;38:703–8.

[29] Hasegawa H, Komura S, Utsunomiya A, Horita Z, Furukawa M, Nemoto M, et al. Thermal stability of ultrafine-grained aluminum in the presence of Mg and Zr additions. Mater Sci Eng A 1999;265:188–96.

[30] Armstrong R, Godd I, Douthwaite RM, Petch NJ. Plastic deformation of polycrystalling aggregates. Philos Mag 1962;7:45–58.

[31] Attallah MM, Davis CL, Strangwood M. Microstructure–microhardness relationship in friction stir welded AA5251. J Mater Sci 2007;42:7299–306.